INTERFACE

rsif.royalsocietypublishing.org

Research

Cite this article: Giverso C, Verani M, Ciarletta P. 2015 Branching instability in expanding bacterial colonies. *J. R. Soc. Interface* **12**: 20141290.
http://dx.doi.org/10.1098/rsif.2014.1290

Received: 21 November 2014
Accepted: 13 January 2015

Subject Areas:
mathematical physics, biophysics

Keywords:
branching instability, bacterial colony growth, pattern formation

Author for correspondence:
Pasquale Ciarletta
e-mail: pasquale.ciarletta@upmc.fr

Electronic supplementary material is available at http://dx.doi.org/10.1098/rsif.2014.1290 or via http://rsif.royalsocietypublishing.org.

THE ROYAL SOCIETY PUBLISHING

Branching instability in expanding bacterial colonies

Chiara Giverso[1,2], Marco Verani[1] and Pasquale Ciarletta[2,3]

[1]MOX, Politecnico di Milano, P.za Leonardo da Vinci, 32, 20133 Milan, Italy
[2]Fondazione CEN, P.za Leonardo da Vinci, 32, 20133 Milan, Italy
[3]CNRS and Sorbonne Universités, Institut Jean le Rond d'Alembert, UPMC Univ Paris 06, UMR 7190, 4 place Jussieu case 162, 75005 Paris, France

Self-organization in developing living organisms relies on the capability of cells to duplicate and perform a collective motion inside the surrounding environment. Chemical and mechanical interactions coordinate such a cooperative behaviour, driving the dynamical evolution of the macroscopic system. In this work, we perform an analytical and computational analysis to study pattern formation during the spreading of an initially circular bacterial colony on a Petri dish. The continuous mathematical model addresses the growth and the chemotactic migration of the living monolayer, together with the diffusion and consumption of nutrients in the agar. The governing equations contain four dimensionless parameters, accounting for the interplay among the chemotactic response, the bacteria–substrate interaction and the experimental geometry. The spreading colony is found to be always linearly unstable to perturbations of the interface, whereas branching instability arises in finite-element numerical simulations. The typical length scales of such fingers, which align in the radial direction and later undergo further branching, are controlled by the size parameters of the problem, whereas the emergence of branching is favoured if the diffusion is dominant on the chemotaxis. The model is able to predict the experimental morphologies, confirming that compact (resp. branched) patterns arise for fast (resp. slow) expanding colonies. Such results, while providing new insights into pattern selection in bacterial colonies, may finally have important applications for designing controlled patterns.

1. Introduction

The collective motion rather than the migration of single individuals is known to drive the macroscopic evolution of many biological processes, such as wound healing [1,2], biofilm formation [3], tumour growth [1,4–6] and morphogenetic processes [1,7–9]. In fact, living cells and bacteria tend to form closely packed clusters (e.g. the columnar structures emerging in expanding living colonies) in which microscopic self-interactions result in cooperative migration [7,10]. Although each individual in a population can determine its own fate, recent findings highlighted that single behaviours and abilities are adjusted, thanks to stochastic differentiation, in order to fit the needs of the population as a whole [11,12].

In order to coordinate such cooperative activities, the chemical and the mechanical interactions both among individual entities and with the extracellular environment are of paramount importance. Chemical communication relies either on the capability of the cells to secrete chemicals (in cell-to-cell chemical signalling) or on the ability to sense an external chemical field, by binding specific signal molecules through their membrane receptors [13]. The chemical interaction can not only occur between adjacent cells, but can also act over long distances, through complex intracellular mechanisms involving signal transduction networks and gene network dynamics [14]. Nevertheless, living matter is not only responding to soluble biochemical signals, but also to physical factors, e.g. through surface cell receptors such as integrins and focal adhesion proteins, establishing a mechanical feedback of fundamental importance in both physiological and pathological conditions [15,16]. Thus, endogenous and exogenous physical

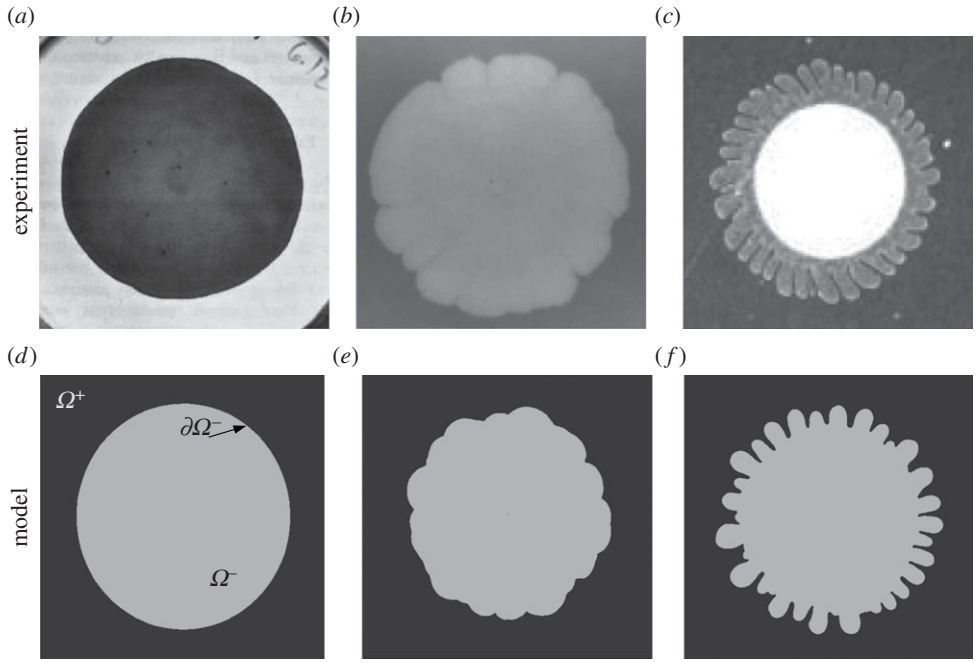

Figure 1. Comparison between some bacterial morphologies observed in biological experiments (*a–c*, reproduced with permission from references [24,23,13], respectively) and the results obtained through the numerical simulations of the proposed mechanical model (*d–f*). The numerical simulations are obtained setting (*d*) $R_0^* = 31$, $R_{out} = 155$, $\beta = 160$ and $\sigma = 0.003$, (*e*) $R_0^* = 70$, $R_{out} = 350$, $\beta = 8.5$ and $\sigma = 0.007$, (*f*) $R_0^* = 100$, $R_{out} = 500$, $\beta = 1$ and $\sigma = 0.007$.

forces act as key regulators of important intracellular signals that drive the dynamical evolution of living organisms through mechanotransduction [17].

In particular, we focus here on pattern formation in expanding bacterial clusters, studying the influence of the chemotactic motility of the colony, the interaction between the bacteria and the substrate as well as the size effects in experiments. A bacterial colony is an excellent biological system model to study general principles of collective motion and pattern formation in complex living organisms [10]. Furthermore, the study of cooperative migration and the onset of branched morphologies in bacterial colonies is an extremely multidisciplinary field of research, combining biological information with the mathematical theories of nonlinear dynamics and the physics and mechanics of non-equilibrium processes.

Thus, bacterial capability to develop elaborate branched patterns, even starting from an initially homogeneous microbial monolayer, has been intensively studied from the biological point of view, plating different bacterial colonies on a Petri dish covered with agar, under different environmental conditions [18–23]. Some of the observed patterns are reported in figure 1*a–c*, ranging from a disc-like colony (figure 1*a*) to a densely branched morphology (figure 1*c*). These biological observations highlight that nutrient diffusion and the interaction with the substrate, together with the cellular capability to proliferate and move either in a random-walk-like fashion or in response to external chemical signals (i.e. chemotaxis), are the key ingredients in the progression of front instabilities.

Indeed, both random and biased flagellation-based, run-and-tumble bacterial motions, in conjunction with collective lubrication by secretion of surfactants, enable rapid colony expansion (i.e. up to centimetres per hour [25]), as extensively studied for many bacterial species. However, we remark for sake of completeness that some bacteria also possess other motility mechanisms for colonization. For example, recent studies on *Paenibacillus dendritiformis* [25] and on myxobacteria [26] have shown that very long bacterial cells do not swarm with the standard dynamic patterns of whirls and jets, but they rather form long tracks in which each individual bacterium periodically reverses its direction, moving back and forth along moderately curved lines. The short time between this direction switching was found to be independent of the number of neighbours and the environmental factors, suggesting the existence of an extraordinary robust internal clock for reversal events in bacteria. Although the evolutionary advantages of such a reversible motion remain unclear and deserve further studies [26], we focus in the following only on the standard run-and-tumble colony expansion.

Many *in silico* mathematical models have been proposed to reproduce the spontaneous onset of the complex patterns observed during microbial growth. The theoretical approaches can be divided into two main categories: hybrid and continuous models. In hybrid models [18,27–30], the microorganisms are represented as discrete, moving entities, whereas the time evolution of the chemicals is described by reaction–diffusion equations. In continuous models [19,22,29,31–34], the bacteria as well as the nutrients and all the other possible factors involved in the process are represented via their density per unit surface. The most popular models of bacterial growth are systems of reaction–diffusion equations [22,23,31–35], allowing the description of colony patterns, including not only spreading disc-like patterns, which was found to be consistent with the solution of a two-dimensional Fisher equation for the bacterial cell density [23,35], but also branched and fractal ones [32,33]. Because bacteria expansion is modelled only by diffusion (i.e. without allowance for chemotaxis), instabilities arise either because of a nonlinear (e.g. density-dependent) diffusion coefficient [22,33] or thanks to the introduction of a bacterial transition from the active-motile and proliferative state to a passive one [31]. Furthermore, the observed branched patterns have been recovered using the assumption of a nutrition-limited process [19,22,24,33,36] or by combining signalling from a chemorepellent and a chemoattractant coupled with a proper dynamic for the colony, e.g. derived from the classical Keller–Segel model [37].

All of these studies have focused on diffusing chemicals as the major driving factors of the process, neglecting any mechanical balance laws. Some efforts to include the mechanical considerations in the modelling of bacterial expansion during the colony expansion have been done in hybrid models [28], having the major drawback of the small number of individuals that can be simulated numerically.

Moreover, the modelling of the viscous interaction between the colony and the substrate has been recently proposed in a continuous model of biofilm formation [3], proving the instability of a bacterial biofilm with planar front whose expansion relies on a nutrient-driven volumetric mass source without any chemotactic motion.

In this work, we investigate the growth and chemotactic mobility of a biological colony, coupled with the diffusion and consumption of nutrients provided by the agar, using a continuum mechanical model at the macroscopic scale. Because bacteria maintain contact with their neighbours and no gaps appear during culture expansion, the continuum assumption is effectively formulated. Moreover, bacterial growth within a Petri dish is described as a free-boundary two-dimensional problem. In the following, we first present the mathematical model based on thermomechanical considerations for describing the expansion of a circular bacterial colony. We later perform the linear stability analysis for the resulting diffusive circular growth, and we study the dynamics of pattern formation in the nonlinear regime using numerical simulations.

2. Mathematical model

A bacterial colony can be modelled as a two-dimensional continuum body occupying a region denoted by Ω^-, with a moving boundary $\partial\Omega^-$ (figure 1*d*). The bacteria are immersed into a spatial outer domain, Ω^+, with boundary $\partial\Omega^+$ that stands for the border of the Petri dish with radius R_{out}. The domain Ω^+ represents the lubricant fluid on the top of the agar, which seems to be collectively produced by the bacteria themselves, although it could also be drawn from the agar during colony expansion [18,19,24].

The mathematical model takes into account the diffusion of the nutrients in the fluid on the top of the agar, the chemotactic mobility of the bacteria and the mechanical interactions with the substrate. Here, we consider a single nutrient species with volume concentration $n(\mathbf{x},t)$, e.g. peptone, diffusing from the outer boundary $\partial\Omega^+$, with diffusion coefficient D_n and consumed, with an uptake rate γ_n, only in the region occupied by the living material, such that

$$\dot{n}(\mathbf{x},t) = \begin{cases} D_n\nabla^2 n(\mathbf{x},t) - \gamma_n n(\mathbf{x},t) & \text{in } \Omega^-, \\ D_n\nabla^2 n(\mathbf{x},t) & \text{in } \Omega^+. \end{cases} \tag{2.1}$$

Considering that the living material can be macroscopically described by a Newtonian fluid moving at low Reynolds numbers [38–40], the classical Darcy's law gives the velocity of the living colony, $\mathbf{v} = -K_p\nabla p$, where K_p is the permeability coefficient describing the friction properties with the substrate and p is the pressure.

Then, assuming that the colony grows, thanks to a non-convective mass flux $\mathbf{m}$, without any significant volumetric mass source, the standard mass balance for the bacterial spatial density ρ reads $\partial\rho/\partial t + \nabla\cdot(\rho\mathbf{v}) = \nabla\cdot\mathbf{m}$. Being bacteria mostly composed by water, the incompressibility constraint leads to $\rho\nabla\cdot\mathbf{v} = \nabla\cdot\mathbf{m}$.

Biological evidence suggests that bacteria are able to implement directional movements, by decreasing the tumbling frequency of their flagella, when they move up the gradient of the chemoattractant [41]. Thus, by neglecting the random motion of bacteria with respect to the directional one, we can assume that the non-convective mass flux vector is directed along the gradient of the chemical concentration, such that $\mathbf{m} = \chi\rho\nabla n$, where χ is the chemotactic coefficient [37]. Substituting Darcy's law in the mass balance equation for a homogeneous microbial colony gives the following relation between the pressure p and the nutrient concentration

$$\nabla^2 p = -\frac{\chi}{K_p}\nabla^2 n \quad \text{in } \Omega^-. \tag{2.2}$$

In order to solve the system of partial differential equations (2.1)–(2.2), boundary conditions are to be provided. In particular, on $\partial\Omega^-$, we apply the Young–Laplace equation for the pressure, the compatibility condition for the moving interface and the classical continuity conditions for the nutrient concentration and its normal derivative

$$p = p_0 - \sigma_b C, \qquad \frac{d\mathbf{x}_{\partial\Omega^-}}{dt}\cdot\mathbf{n} = \mathbf{v}_{\partial\Omega^-}\cdot\mathbf{n} \tag{2.3}$$

and

$$[\![n]\!]_{\partial\Omega^-} = 0, \qquad [\![\nabla n\cdot\mathbf{n}]\!]_{\partial\Omega^-} = 0, \tag{2.4}$$

where C is the local curvature of the free boundary, σ_b is the surface tension of the interface, p_0 is the constant outer pressure and $\mathbf{n}$ is the outward normal vector at the boundary. It is worth noting that the surface tension of the bacterial colony results from the collective interaction with the biopolymers forming the surrounding liquid environment [42].

In the following, we apply this model to a initially circular bacterial colony of radius $R_0^* = R^*(t=0)$, deriving the non-dimensional system of governing equations for the dimensionless chemical concentration, $\bar{n}$, and the dimensionless pressure, $\bar{p}$

$$\dot{\bar{n}} = \begin{cases} \nabla^2\bar{n} - \bar{n} & \text{in } \Omega^- \\ \nabla^2\bar{n} & \text{in } \Omega^+ \end{cases} \tag{2.5}$$

and

$$\nabla^2\bar{p} = -\beta\nabla^2\bar{n} \quad \text{in } \Omega^-, \tag{2.6}$$

using the following characteristic time t_c, length l_c, velocity v_c, pressure p_c and chemical concentration n_c: $t_c = \gamma_n^{-1}$, $l_c = \sqrt{D_n\gamma_n^{-1}}$, $v_c = \sqrt{D_n\gamma_n}$, $p_c = D_nK_p^{-1}$, $n_c = n|_{R_{\text{out}}}$, where $n|_{R_{\text{out}}}$ is the fixed concentration at the outer border of the Petri dish. The dimensionless boundary conditions for the pressure, the chemical concentration of the nutrients and the velocity, on the colony front $\partial\Omega^-$, read

$$\bar{p} = \bar{p}_0 - \bar{\sigma}\bar{C} \tag{2.7}$$

$$[\![\bar{n}]\!]_{\partial\Omega^-} = 0, \qquad [\![\nabla\bar{n}\cdot\mathbf{n}]\!]_{\partial\Omega^-} = 0 \tag{2.8}$$

and

$$\frac{d\bar{\mathbf{x}}_{\partial\Omega^-}}{dt}\cdot\mathbf{n} = \bar{\mathbf{v}}_{\partial\Omega^-}\cdot\mathbf{n}. \tag{2.9}$$

On the other hand, the boundary condition on the nutrient concentration on $\partial\Omega^+$ is given by $\bar{n}(t, R_{\text{out}}) = 1$. For the sake of simplicity, we omit in the following the barred notation to denote dimensionless quantities.

The non-dimensionalization procedure leads to the definition of four dimensionless parameters: two of them, $\beta := \chi n_c/D_n$ and $\sigma := \sigma_b K_p\gamma_n^{1/2}D_n^{-3/2}$ are related to the chemotactic response and the bacteria–substrate interaction

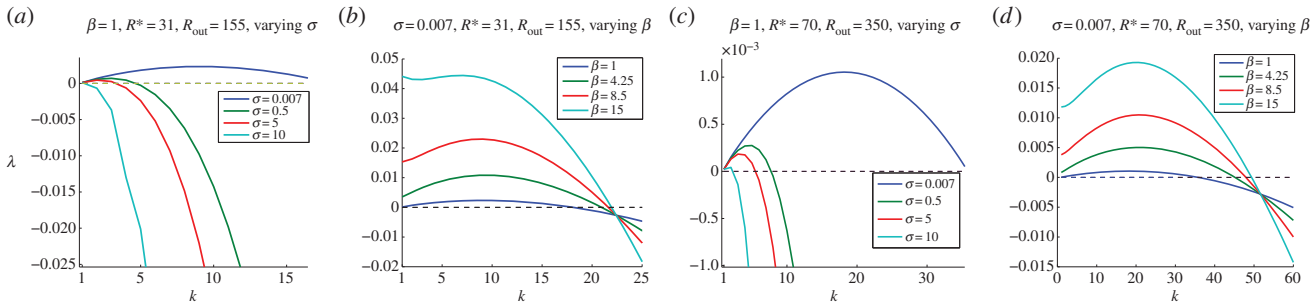

Figure 2. Dispersion diagrams, varying (*a*,*c*) σ and (*b*,*d*) β, for a colony of radius $R^* = 31$ in a Petri dish of radius $R_{out} = 155$ in (*a*,*b*) and a colony of radius $R^* = 70$ in a Petri dish of radius $R_{out} = 350$ in (*c*,*d*). For the sake of graphic clarity, the solid lines are obtained by interpolating the discrete values of λ obtained from the numerical solution of the dispersion equations (3.1) for the integer values of $k \in N^+$. (Online version in colour.)

(*motility* parameters), whereas the other two, R_0^* (i.e. dimensionless initial radius of the circular colony) and R_{out} (i.e. the dimensionless outer radius of the Petri dish) define the geometrical properties of the system with respect to the diffusive length, l_c (*size* parameters). In particular, the dimensionless parameter β represents the ratio between the energy required for the chemotactic expansion of the colony and the energy provided by the diffusive nutrients, whereas considering that K_p can be related to the friction between the colony and the substrate, ζ, through $K_p = l_c/\zeta$, the dimensionless parameter σ becomes the ratio between the surface tension of the bacterial colony and the product of the colony–substrate friction and the diffusion coefficient, i.e. $\sigma = \sigma_b/(D_n\zeta)$.

3. Results

3.1. Linear stability analysis

The linear stability analysis for standard problems with a moving interface is usually performed by perturbing a steady state or a steady wave profile in a comoving frame, such as travelling wave solutions for infinite rectilinear fronts. Because the governing equations for the finite bacterial domain do not admit such kinds of solution for a circular front, let us consider the quasi-stationary expansion of a circular bacterial colony of radius $R^*(t)$, assuming that the diffusive process is much faster than the border expansion, so that the time-derivative term in (2.5) can be neglected. The quasi-stationary velocity of the circular front has only a radial component, i.e. $\mathbf{v}^* = v_r^*\mathbf{e}_r$, with $v_r^* = \beta n_0 I_1(R^*)/I_0(R^*)$, where $I_j(r)$ is the modified Bessel function of the first kind of order j, evaluated in r, and $n_0 = (1 + I_1(R^*)/I_0(R^*)R^* \log(R_{out}/R^*))^{-1}$ is the nutrient concentration at the free boundary, in the quasi-stationary state. Further details on the derivation of the quasi-stationary solution are presented in the electronic supplementary material.

Considering a perturbation of the moving interface given by $R(\theta, t) = R^*(t) + \varepsilon e^{\lambda t + ik\theta}$, it is possible to find the dispersion equation relating the time growth rate λ to the integer wavenumber k in an implicit way, as a function of the four dimensionless parameters β, σ, R^* and R_{out}

$$\lambda = -\frac{\sigma}{R^{*3}}(k^3 - k) + \beta A_\lambda \sqrt{\lambda + 1} I_{k+1}\left(\sqrt{\lambda + 1}R^*\right) - \beta n_0 \left((1 + k)\frac{I_1(R^*)}{R^* I_0(R^*)} - 1\right), \tag{3.1}$$

for $\lambda \neq -1$. More information on the procedure used to obtain the dispersion relations and the determination of the coefficient A_λ can be found in the electronic supplementary material.

Interestingly, equation (3.1) shows that the amplification rate of the perturbation over time depends on the radius of the colony, R^*. The dispersion diagrams presented in figure 2, obtained solving iteratively the dispersion equation (3.1) through the secant method, demonstrate that the colony boundary is always linearly unstable for large wavelengths. The resulting dispersion curves show a stabilization of the front at short-wavelengths, which is also typically found in some classical fluid instabilities [43]. Indeed, the governing equations closely resemble those driving the Saffman–Taylor instability in a Hele–Shaw cell, where σ has the same physical meaning of the capillary number, introducing a correction in the dispersion relation proportional to $(k - k^3)$ [44]. Such a regularizing effect is even enforced in our model by the presence of the Laplacian operator at the right-hand side of equation (2.2), corresponding to a mass source term which is not considered in viscous instabilities. While for a planar front, one would expect to find $\lambda = 0$ for $k = 0$ for translational symmetry, we note that for the circular front we consider $k \in \mathbb{N}^+$, because $k = 0$ would correspond to the quasi-static expansion of the circular front. Furthermore, even if β somewhat physically corresponds to the influx volume flow rate in an initially circular front, the velocity of the quasi-stationary front depends in this problem on the initial radius R^*, while it is often taken as a constant in viscous fingering problems [45], thus introducing a marked size-dependence in the resulting dispersion equation. In both cases, the linear stability analysis can identify the finite critical (or characteristic) wavelength with the most unstable growth rate, which increases for increasing β. Nonetheless, even if such linear stability curves are indicative of unstable front dynamics, suggesting the nonlinear formation of dendritic patterns [46], we also expect to find differences in the fully nonlinear dynamics owing to the more complex functional dependence on the growth and geometrical parameters in this problem. Furthermore, the maximum time growth rate increases as far as β increases, as shown in figure 2*b*,*d*. Comparing the dispersion curves for different dimensionless radii of the colony, while maintaining the ratio between R^* and R_{out} as a constant (which corresponds to a variation of the diffusive length), it is possible to note that increasing such a size parameter increases the range of unstable wavenumbers and the characteristic wavenumber, but it decreases the value of the fastest growth rate (figure 2*b* versus *d*).

3.2. Numerical simulations

Because the linear analysis indicates the occurrence of a front instability with a finite characteristic wavenumber, we investigate the nonlinear pattern formation of the bacterial

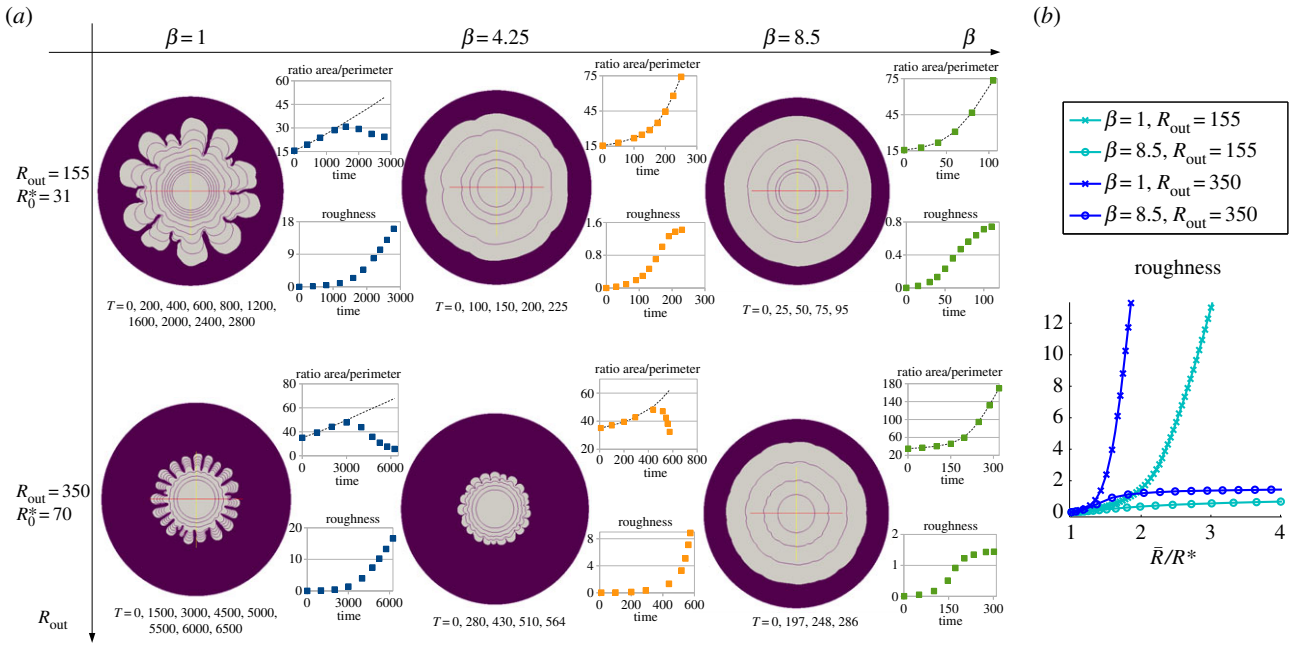

Figure 3. Morphological diagram of the expanding bacterial colony for different values of β and R_{out} in the numerical simulations, setting $\sigma = 0.007$ and $R_{out}/R_0^* = 5$ fixed. (*a*) The contour of the colony is plotted at different instants of time. The top-right charts report the area/perimeter ratio of the bacterial colony (square markers) and half of the averaged radius of the colony (dashed lines), whereas the bottom-right charts depict the roughness of the interface over time. (*b*) Roughness of the colony contour for different values of the parameters β and R_{out}, over the normalized averaged radius of the colony. Branched patterns show a continuously increasing roughness, which in turn saturates for rounder colonies. The dynamic plots of the chemical concentration and the pressure fields are reported in the electronic supplementary material, movies S1 and S2 for the particular case $\beta = 1$, $R_{out} = 155$, $R_0^* = 31$. (Online version in colour.)

colony using a finite-element code implemented in FreeFem++ (http://www.freefem.org). The equations (2.5)–(2.6) are solved on an adaptively refined triangular grid, fitting the moving interface. Given the concentration of nutrients at time t_i, we first compute the pressure p_i, through equation (2.6) and then the velocity field, using Darcy's law. We are yet able to explicitly move the boundary and solve (2.5) for the concentration at time t_{i+1}, using an implicit-Euler scheme.

The numerical results are reported in figure 3*a* showing the emerging patterns versus the two dimensionless parameters β and R_{out}, at fixed R_{out}/R_0^* and σ.

In particular, it is found that the branching of the colony is strongly favoured by smaller values of the motility parameter β. Because β drives the velocity of the quasi-stationary front, we find that the instability of the contour is enhanced by a low expanding velocity, which is a common feature of growing biological systems in a diffusion-dominated regime [5]. In fact, small values of β correspond to situations in which the diffusion of chemicals is dominant on the chemotactic mobility of the colony.

Furthermore, figure 3*a* points out the existence of a size effect in pattern formation, showing that the size parameter R_{out} determines the characteristic wavelength of the branching process. In fact, keeping the aspect ratio R_{out}/R_0^* constant, a larger Petri dish R_{out}, with respect to the diffusive length l_c, determines branched patterns characterized by a smaller wavenumber.

The morphological diagram in figure 3*a* also reveals that the number of emerging fingers perfectly corresponds to the critical wavenumbers predicted by the linear stability analysis. Indeed, for the particular case $\beta = 1$, $R_0^* = 31$ and $R_{out} = 155$, the blue dispersion curves in figure 2*a*,*b* predict the fastest linearly unstable mode with $k_c = 10$, whereas in the numerical simulations (figure 3*a* top-right), 10 branches can be observed. Moreover, for $\beta = 1$, $R_0^* = 70$ and $R_{out} = 350$, the analytical characteristic wavenumber (see the blue dispersion curves in figure 2*c*,*d*) is $k_c = 19$, which is confirmed by the numerical simulation in figure 3*a* bottom-right, where 19 totally developed branches appear. Considering $\beta = 4.25$, the maximum in the red dispersion curve in figure 2*d* shifts to $k_c = 22$, which is in agreement with the 22 fingers depicted in figure 3*a* bottom-centre, where the same parameters are considered. The agreement between numerical and analytical results is good whenever the velocity of the front is slow enough to satisfy the quasi-stationary hypothesis, suggesting that in this regime the nonlinear effects fix the linearly unstable pattern. Conversely, the nonlinearities have a much stronger stabilizing effect on the colony profile when considering initially fast front dynamics, corresponding to high values of the parameter β. This fully nonlinear behaviour is strikingly similar to the diffusion-dominated instability in other biological systems, where rounder patterns are observed for increasingly faster initial fronts [5].

The morphological diagram in figure 3*a* also highlights that the occurrence of branching can be detected when the ratio between the area of the colony and its perimeter over time (square markers) deviates from half of the average radius of the colony (dashed lines).

Another important parameter in the definition of branched patterns is the roughness of the profile, measured as the root of the mean square deviation of points on the front from the average radius of the colony [29]. Either plotting this parameter as a function of time (figure 3*a*) or as a function of the averaged radius of the colony, $\bar{R}$, normalized with respect to the initial radius, R_0^* (figure 3*b*), it is possible to observe that the interface roughness continuously increases for branched patterns, whereas it later saturates to an almost constant value only in compact colonies, in agreement with the experimental measurements performed in

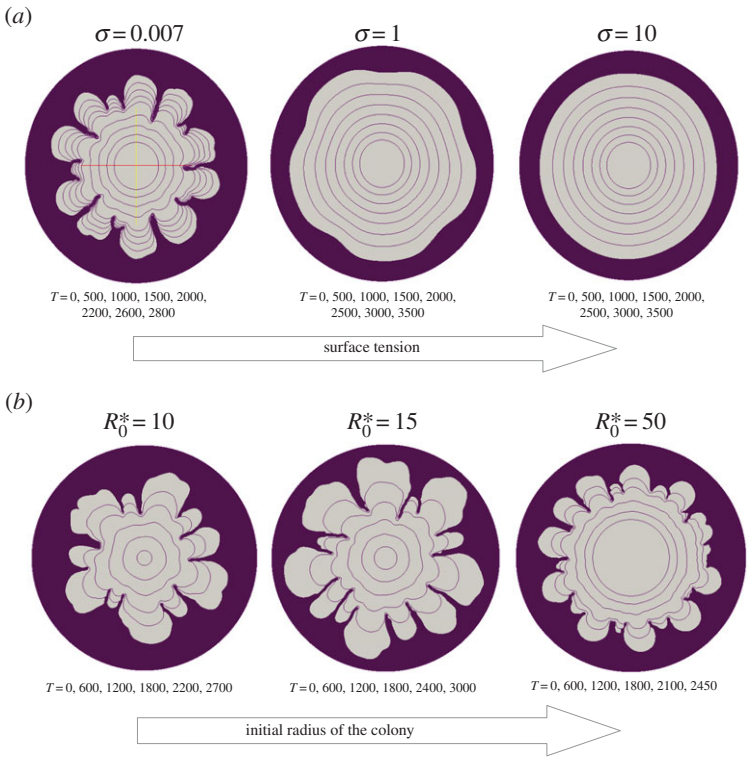

Figure 4. Influence of (*a*) the parameter σ and (*b*) the initial radius R_0^* on the formation of contour instabilities. (*a*) The surface tension has a stabilizing effect on the motion of the free boundary. The simulations were obtained imposing $R_{out} = 155$, $R_0^* = 31$ and $\beta = 1$. The dynamic plots of the contours are reported in the electronic supplementary material, movies S3–S5. (*b*) The number of fingers that develop increases as the radius of the colony is bigger. The simulations were obtained imposing $R_{out} = 155$, $\sigma = 0.007$ and $\beta = 1$. (Online version in colour.)

reference [47]. In summary, it is found that the motility parameter β defines the occurrence of the branching regime, whereas the size parameter R_{out} determines the characteristic wavelength of the branching process.

Furthermore, numerical simulations agree with the theory in predicting that an increase of the surface tension σ has a stabilizing effect also in the nonlinear regime (figure 4*a* and the electronic supplementary material, movies S3–S5). Another important parameter in the model is the initial size of the colony R_0^*, with respect to the diffusive length. In order to assess the influence of this parameter on the onset of branches, we have run a set of simulations keeping R_{out}, σ and β fixed and letting R_0^* vary. The resulting morphological diagram is reported in figure 4*b*, showing that more fingers develop as the initial radius of the colony increases.

Let us now briefly discuss the characteristics of the branching process in the expanding colony. Once branching has been triggered, all developing fingers elongate in the radial direction. Further branching can occur, even though some of the second-generation fingers remain very short because of the geometrical constraints imposed by their neighbours. In figure 5, the geometrical characteristics of the fingers are plotted versus time. We define the finger base, B, as the distance between two subsequent points of local maximum for the curvature of the moving front. The amplitude of the finger, A, is defined as the maximum distance between the points belonging to the finger contour and the corresponding finger base segment. The numerical results in figure 5 correspond to the simulation on the upper left of figure 3. It is observed that at an early stage (up to $t = 1650$) both the amplitude and the base strongly increase for each of the five evolving fingers. As soon as second-generation fingers appear (from $t = 1650$ on), the amplitude of the new ones strongly increases, whereas the base remains almost constant in time. We report in the table within figure 5 the parameters of the power-law curve, $c \cdot t^{\alpha}$, which best fits the numerical data for the base and the amplitude of the fingers. Interestingly, at the early stage, the best-fitting exponent for the ratio amplitude/base of the fingers is ≈0.45, which is very close to the expected square root growth over time exponent in a diffusion-driven instability [43].

Let us now return to the dimensional physical quantities in order to discuss the results of the numerical simulations with respect to the biological data. Available data in experimental literature for expanding colonies are shown in table 1. In particular, in the following, we compare the results of the simulated patterns of our model, reported in figure 1*d–f*, with their corresponding experimental counterparts in figure 1*a–c*. In all cases, the Petri dishes in the experiments have the standard radius of 44 mm.

As shown in figure 1*d*, the evolution of the disc-like colony observed in reference [24] can be reproduced by taking a diffusion coefficient $D_n = 3 \times 10^{-11}\ \mathrm{m^2\,s^{-1}}$, and a small uptake rate, $\gamma = 3.7 \times 10^{-4}\ \mathrm{s^{-1}}$, giving a characteristic length $l_c \approx 285\ \mu\mathrm{m}$, corresponding to a dimensionless external radius of $R_{out} \approx 155$. Fixing $\beta = 8.5$, we obtain an average velocity of the front equal to $\approx 3.2\ \mathrm{mm\,h^{-1}}$, which is in the order of magnitude of the values found in literature for round and compact colonies, such as the one in figure 1*a* (table 1). Considering the characteristic concentration $c_n = 0.1$ mM, as the one used in reference [48], the parameter $\beta = 8.5$ describes a chemotactic coefficient $\chi \approx 48 \times 10^{-5}\ \mathrm{cm^2/(s\,mM)}$, which is also in the biological range (table 1).

Thus, disc-like patterns are found to arise in situations in which the chemicals have an intermediate diffusion rate and are consumed by bacteria at a slow rate. Moreover, an

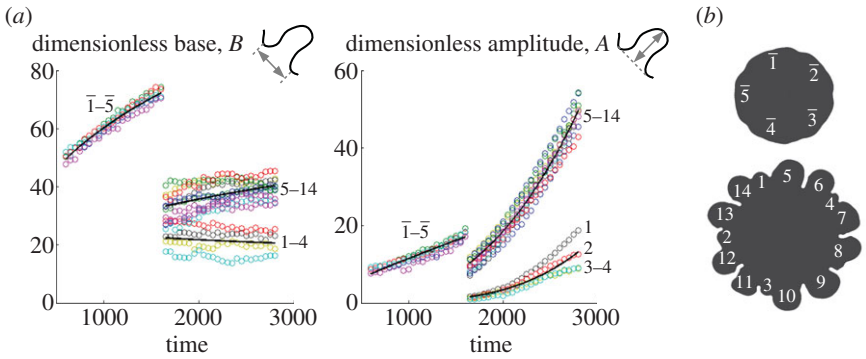

(c)

fit. ct^{α}	c	α
B ($\bar{1}$–$\bar{5}$)	4.18	0.386
A ($\bar{1}$–$\bar{5}$)	0.036	0.83
B (1–14)	71.2 (1–4); 2.3 (5–14)	–0.16 (1–4); 0.36 (5–14)
A (1–14)	1.9×10^{-13} (1–4); 3×10^{-9} (5–14)	4.0 (1–4); 2.9 (5–14)

Figure 5. Fingers' base and amplitude in the case $\beta = 1$, $R_{out} = 155$, $R_0^* = 31$, $\sigma = 0.007$. (*a*) Base and amplitude of fingers (circles): up to time $t = 1650$, five principal fingers develop, then tip-splitting occurs and 14 fingers emerge. (*b*) Numbering of the fingers considered in the simulation. (*c*) Table reporting the fitting parameters of the data with a power-law curve of the kind ct^{α} (solid lines). (Online version in colour.)

Table 1. Biologically meaningful ranges for the parameters of the model.

	values	refs
D_n	10^{-11}–10^{-9} $m^2 s^{-1}$	[3,24,48,49]
γ_n	10^{-4}–10^{-3} s^{-1}	[50]
v_{colony}	60–400 μm h^{-1} (finger);	[13,22]
	60–300 μm h^{-1} (Eden);	[22,31]
	4–18 mm h^{-1} (disc)	
σ_b	0.07 nN μm^{-1}	[51]
ζ	1–10^2 nNs/(μm^3)	[52]
χ	3.75–188 × 10^{-5} cm^2/(s mM)	[48,53]

Eden-like pattern (i.e. a clusters whose inner structure is almost completely compact but whose surface is comparatively rough [23]) is observed considering a smaller diffusion coefficient $D_n = 10^{-11}$ m^2 s^{-1} [24] and an uptake rate $\gamma = 6.5 \times 10^{-4}$ s^{-1} (i.e. $l_c \approx 124$ μm and $v_c \approx 290$ μm h^{-1}, $R_{out} \approx 350$) as depicted in figure 1*e*. Keeping $\beta = 8.5$, the resulting mean front velocity is equal to 136 μm h^{-1}, which is in agreement with the reported velocities for such patterns (table 1). In this case, under the same assumptions used above, we obtain a consistent chemotactic coefficient of about $\chi \approx 0.85 \times 10^{-5}$ cm^2/(s mM). Therefore, our model predicts that Eden-like structures can be obtained in the range of relatively small diffusion coefficients of the nutrients, intermediate uptake rates and small chemotactic behaviour. Although reproducing the typical macroscopic roughness of a compact colony, we have to remark that our continuous model is not able to capture the observed microscopic roughness [31], which would require a discrete approach at a cellular scale.

Furthermore, we have found that branched structures arise in simulations with high values of the dimensionless external radius R_{out} and small values of the motility parameter β, physically corresponding to high values of both nutrient diffusion and uptake rate, coupled with a low concentration of nutrients in the agar. Indeed, the development and evolution of the fingers reported in reference [13] are reproduced by our simulations in figure 1*f*, considering $\gamma = 0.11$ s^{-1} and $D_n = 10^{-10}$ m^2 s^{-1}, so that $l_c \approx 30$ μm and $t_c \approx 9$ s. Accordingly, the observed displacement of about 2.4 mm in the first 22 h, for an initial colony with a diameter of about 6 mm [13], perfectly corresponds to the displacement of the front recorded in this simulation (i.e. $82 \cdot l_c$ at $T = 9000$, for a colony with $R_0^* = 100$). In this case, we fix $\beta = 1$, corresponding to a chemotactic coefficient $\chi \approx 10^{-5}$ cm^2/(s mM), which is slightly below the typical values reported in reference [48].

In summary, our model is able to predict the observed experimental morphologies, reproducing that higher velocities of the front, which are linked to a stronger response of bacteria to the external chemical field (i.e. high χ), correspond to more rounded profiles, in accordance with biological observations [22,31].

Let us finally add a few considerations about the role of surface tension for pattern formation. Considering a friction coefficient $\zeta = 1$ nNs/(μm) (compatible with the values reported in table 1), the surface tension for the three simulations results in the range $\sigma_b \approx 0.09$–0.7 nN μm^{-1}, which is slightly higher than the values found for cell clusters (table 1). Accordingly, although we find that disc-like colonies can also be numerically obtained by increasing the dimensionless motility parameter σ (figure 4), this would correspond to much higher values of the surface tension than the biological range. In conclusion, we argue that the compact expansion of the bacterial front likely relies more on the capability of bacteria to actively move and consume nutrients and on the diffusive properties of the chemicals in the agar, rather than on the surface tension and the adhesive properties of the colony.

4. Discussion

In this work, we have presented an analytical and computational analysis of a continuum model for studying pattern

formation during the spreading of an initially circular bacterial colony on a Petri dish. The proposed model differs from previous ones [3,23,33] by taking into account both the chemical effects, dictated by the diffusion of nutrients and the chemotactic response of bacteria, and the mechanical/viscous interaction between the colony and the substrate. In particular, four dimensionless parameters are found to characterize the model dynamics: two of them describe the factors that drive the *motility* of the colony, i.e. β represents the competition between chemotactic and diffusive effects, whereas σ is the ratio between the surface tension of the colony and the friction with the substrate, whereas the initial dimensionless radius of the colony, R_0^*, and the dimensionless radius of the Petri dish, R_{out}, account for *size* effects.

The linear stability analysis has evidenced that an initially circular colony is always linearly unstable to perturbations of the interface, having the typical dispersion curves found for fluid instabilities, such as viscous fingering. The numerical simulations of bacterial spreading in the fully nonlinear regime have confirmed the development of undulated finger-like structures, which align in the radial direction and later undergo further branching, and the existence of a characteristic wavenumber, as predicted by the linear stability analysis. While the finger dynamical behaviour shows the occurrence of the typical shielding and tip-splitting found in Saffman–Taylor instability [44], we find here a more complex dependence of the characteristic length scales of such fingers on the size parameters of the problem, with more branched patterns appearing with larger Petri dishes, whereas the emergence of branching is driven by the motility parameters, being especially favoured by small values of σ and β, which also correspond to slow moving fronts. However, through comparison of the model parameters with real biological data, we argue that the selection mechanism of branched patterns likely relies on the *motility* parameter β, i.e. on the interplay between diffusion and chemotaxis, rather than on σ. In particular, in such a range, the aspect ratio of the fingers is found to scale to approximately the square root of the time. Because β drives the velocity of the colony interface, the model also confirms the experimental observations that compact (resp. branched) patterns arise for fast (resp. slow) expanding colonies [22,31]. Furthermore, the scaling laws for the roughness coefficient of the interface in numerical simulations are consistent with the ones reported in the biological investigations [35].

Interestingly, the modelling of the branching structures does not require neither the introduction of a nonlinear (e.g. density-dependent) diffusion coefficient, as in references [22,33,54], nor the transition from the active-motile and proliferative state of bacteria to a passive state, as in reference [31].

The experimental morphologies reported in references [13,23,24] (figure 1*a–c*) are also compared with the patterns resulting from the numerical simulations of the proposed model (figure 1*d–f*), where the relevant biological parameters in each experimental setting are used as input. A striking similarity has been found between experiments and model simulations either on the emerging disc-like, Eden-like and branched structures, or on the pattern dynamics during the expansion process.

It is worth noting that the proposed model is not able to reproduce the evolution of colonies in which fractal patterns or microscopic roughness appear, because other effects should be taken in account at scales where a continuous representation of the colony is no longer a valid assumption. Alternatively, highly fractal patterns can be reproduced by using either reaction–diffusion models with nonlinear terms [24,32,33] or discrete/hybrid models [18,29].

In conclusion, the results of this study suggest that the pattern selection and evolution in expanding bacterial colonies is driven by a complex interplay of the chemotactic response, the substrate–bacteria interaction and the size effects. Furthermore, the present study highlights the necessity to perform new experimental tests with a better quantitative characterization of both the chemical response and the mechanical forces involved during the bacterial expansion, as done for eukaryotic cells [55,56]. Indeed, even if the formation of spatial patterns in growing bacterial colonies has been intensely studied during the last years, further progress in the field has been hindered by the lack of detailed experimental data [10]. Such a combined approach has the potential to foster our understanding of pattern selection and dynamics in bacterial colonies, with important applications for designing and engineering controlled patterns.

Future works will be focused on the refinement of the proposed model, simulating more realistic initial and boundary conditions, possibly supported by novel biological experiments and coupled with a more complex representation for the living material (e.g. including viscoelasticity [57]). Further developments should also include the active motility and the chemomechanical interactions occurring at the microscopic scale inside the colony, which are of fundamental importance in the appearance and evolution of patterns in some bacterial strains [10,25,26].

Finally, future applications of this model shall concern free-boundary problems in other biological systems (e.g. wound healing), aiming at giving insights on the role played by physical forces in directing self-organization during the development of living organisms.

Acknowledgement. We are grateful to Davide Ambrosi for helpful discussions.

Funding statement. This work was partially supported by the 'Start-up Packages and PhD Programme' project, co-funded by Regione Lombardia through the 'Fondo per lo sviluppo e la coesione 2007–2013-formerly FAS' and by the 'Progetto Giovani GNFM 2014', funded by the National Group of Mathematical Physics (GNFM-INdAM).

References

1. Friedl P, Hegerfeldt Y, Tusch M. 2004 Collective cell migration in morphogenesis and cancer. *Int. J. Dev. Biol.* **48**, 441–449. (doi:10.1387/ijdb.041821pf)
2. Poujade M, Grasland-Mongrain E, Hertzog A, Jouanneau J, Chavrier P, Ladoux B, Buguin A, Silberzan P. 2007 Collective migration of an epithelial monolayer in response to a model wound. *Proc. Natl Acad. Sci. USA* **104**, 15 988–15 993. (doi:10.1073/pnas.0705062104)
3. Dockery J, Klapper I. 2001 Finger formation in biofilm layers. *SIAM J. Appl. Math.* **62**, 853–869.

4. Byrne HM. 1999 A weakly nonlinear analysis of a model of avascular tumor growth. *J. Math. Biol.* **39**, 59–89. (doi:10.1007/s002850050163)
5. Ben Amar M, Chatelain C, Ciarletta P. 2011 Contour instabilities in early tumor growth models. *Phys. Rev. Lett.* **106**, 148101. (doi:10.1103/PhysRevLett.106.148101)
6. Greenspan HP. 1976 On the growth and stability of cell cultures and solid tumors. *J. Theor. Biol.* **56**, 229–243. (doi:10.1016/S0022-5193(76)80054-9)
7. Weijer CJ. 2009 Collective cell migration in development. *J. Cell Sci.* **122**, 3215–3223. (doi:10.1242/jcs.036517)
8. Martin P, Parkhurst SM. 2004 Parallels between tissue repair and embryo morphogenesis. *Development* **131**, 3021–3034. (doi:10.1242/dev.01253)
9. Murray JD, Oster GF, Harris AK. 1983 Mechanical aspects of mesenchymal morphogenesis. *J. Embryol. Exp. Morph.* **78**, 83–125.
10. Zhang HP, Beer A, Florin EL, Swinney HL. 2010 Collective motion and density fluctuations in bacterial colonies. *Proc. Natl Acad. Sci. USA* **107**, 13 626–13 630. (doi:10.1073/pnas.1001651107)
11. Ben-Jacob E, Schultz D. 2010 Bacteria determine fate by playing dice with controlled odds. *Proc. Natl Acad. Sci. USA* **107**, 13 197–13 198. (doi:10.1073/pnas.1008254107)
12. Friedl P, Gilmour D. 2009 Collective cell migration in morphogenesis, regeneration and cancer. *Nat. Rev. Mol. Cell Biol.* **10**, 445–457. (doi:10.1038/nrm2720)
13. Be'er A, Zhang HP, Florin EL, Payne SM, Ben-Jacob E, Swinney HL. 2009 Deadly competition between sibling bacterial colonies. *Proc. Natl Acad. Sci. USA* **106**, 428–433. (doi:10.1073/pnas.0811816106)
14. Manz BN, Groves JT. 2010 Spatial organization and signal transduction at intercellular junctions. *Nat. Rev. Mol. Cell Biol.* **11**, 342–352. (doi:10.1038/nrm2883)
15. DuFort CC, Paszek MJ, Weaver VM. 2011 Balancing forces: architectural control of mechanotransduction. *Nat. Rev. Mol. Cell Biol.* **12**, 308–319. (doi:10.1038/nrm3112)
16. Stylianopoulos T *et al*. 2012 Causes, consequences, and remedies for growth-induced solid stress in murine and human tumors. *Proc. Natl Acad. Sci USA* **109**, 15 101–15 108. (doi:10.1073/pnas.1213353109)
17. Ingber DE. 2006 Cellular mechanotransduction: putting all the pieces together again. *FASEB J.* **20**, 811–827. (doi:10.1096/fj.05-5424rev)
18. Ben-Jacob E, Cohen I, Gutnick DL. 1998 Cooperative organization of bacterial colonies: from genotype to morphotype. *Annu. Rev. Microbiol.* **52**, 779–806. (doi:10.1146/annurev.micro.52.1.779)
19. Ben-Jacob E, Cohen I, Levine H. 2000 Cooperative self-organization of microorganisms. *Adv. Phys.* **49**, 395–554. (doi:10.1080/000187300405228)
20. Fujikawa H, Matsushita M. 1989 Fractal growth of *Bacillus subtilis* on agar plates. *J. Phys. Soc. Jpn* **58**, 3875–3878. (doi:10.1143/JPSJ.58.3875)
21. Fujikawa H. 1994 Diversity of the growth patterns of *Bacillus subtilis* colonies on agar plates. *FEMS Microbiol. Ecol.* **13**, 159–168. (doi:10.1111/j.1574-6941.1994.tb00062.x)
22. Kawasaki K, Mochizuki A, Matsushita M, Umeda T, Shigesada N. 1997 Modeling spatio-temporal patterns generated by *Bacillus subtilis*. *J. Theor. Biol.* **188**, 177–185. (doi:10.1006/jtbi.1997.0462)
23. Matsushita M, Hiramatsu F, Kobayashi N, Ozawa T, Yamazaki Y, Matsuyama Y. 2004 Colony formation in bacteria: experiments and modeling. *Biofilms* **1**, 305–317. (doi:10.1017/S1479050505001626)
24. Golding I, Kozlovsky Y, Cohen I, Ben-Jacob E. 1998 Studies of bacterial branching growth using reaction–diffusion models for colonial development. *Physics A* **260**, 510–554. (doi:10.1016/S0378-4371(98)00345-8)
25. Be'er A, Strain SK, Hernández RA, Ben-Jacob E, Florin EL. 2013 Periodic reversals in *Paenibacillus dendritiformis* swarming. *J. Bacteriol.* **195**, 2709–2717. (doi:10.1128/JB.00080-13)
26. Wu Y, Kaiser AD, Jiang Y, Alber MS. 2009 Periodic reversal of direction allows myxobacteria to swarm. *Proc. Natl Acad. Sci. USA* **106**, 1222–1227. (doi:10.1073/pnas.0811662106)
27. Ben-Jacob E, Levine H. 2006 Self-engineering capabilities of bacteria. *J. R. Soc. Interface* **3**, 197–214. (doi:10.1098/rsif.2005.0089)
28. Farrell FDC, Hallatschek O, Marenduzzo D, Waclaw B. 2013 Mechanically driven growth of quasi-two dimensional microbial colonies. *Phys. Rev. Lett.* **111**, 168101. (doi:10.1103/PhysRevLett.111.168101)
29. Bonachela JA, Nadell CD, Xavier JB, Levin SA. 2011 Universality in bacterial colonies. *J. Stat. Phys.* **144**, 303–315. (doi:10.1007/s10955-011-0179-x)
30. Picioreanu C, van Loosdrecht MC, Heijnen JJ. 1998 A new combined differential-discrete cellular automaton approach for biofilm modeling: application for growth in gel beads. *Biotechnol. Bioeng.* **57**, 718–731. (doi:10.1002/(SICI)1097-0290(19980320)57:6<718::AID-BIT9>3.0.CO;2-0)
31. Matsushita M, Wakita J, Itoh H, Ràfols I, Matsuyama T, Sakaguchi H, Mimura M. 1998 Interface growth and pattern formation in bacterial colonies. *Physics A* **249**, 517–524. (doi:10.1016/S0378-4371(97)00511-6)
32. Kozlovsky Y, Cohen I, Golding I, Eshel Ben-Jacob E. 1999 Lubricating bacteria model for branching growth of bacterial colonies. *Phys. Rev. E, Stat. Phys. Plasmas Fluids Relat. Interdiscip. Top.* **59**, 7025–35.
33. Mimura M, Sakaguchi H, Matsushita M. 2000 Reaction–diffusion modelling of bacterial colony patterns. *Physics A* **282**, 283–303. (doi:10.1016/S0378-4371(00)00085-6)
34. Marrocco A, Henry H, Holland IB, Plapp M, Sé ror SJ, Perthame B. 2010 Models of self-organizing bacterial communities and comparisons with experimental observations. *Math. Model. Nat. Phenom.* **5**, 148–162. (doi:10.1051/mmnp/20105107)
35. Wakita J, Komatsu K, Nakahara A, Matsuyama T, Matsushita M. 1994 Experimental investigation on the validity of population dynamics approach to bacterial colony formation. *J. Phys. Soc. Jpn* **63**, 1205–1211. (doi:10.1143/JPSJ.63.1205)
36. Korolev KS, Müller MJI, Karahan N, Murray AW, Hallatschek O, Nelson DR. 2012 Selective sweeps in growing microbial colonies. *Phys. Biol.* **9**, 026008. (doi:10.1088/1478-3975/9/2/026008)
37. Keller EF, Segel LA. 1971 Model for chemotaxis. *J. Theor. Biol.* **30**, 225–234. (doi:10.1016/0022-5193(71)90050-6)
38. Graziano L, Preziosi L. 2007 Mechanics in tumor growth. In *Modeling of biological materials* (eds F Mollica, KR Rajagopal, L Preziosi), pp. 267–328. Boston, MA: Birkhäuser.
39. Lega J, Passot T. 2003 Hydrodynamics of bacterial colonies: a model. *Phys. Rev. E* **67**, 031906. (doi:10.1103/PhysRevE.67.031906)
40. Verdier C, Etienne J, Duperray A, Preziosi L. 2009 Review. Rheological properties of biological materials. C.R. Acad. Sci. *Ser. IV-Physics* **10**, 790–811.
41. Adler J. 1966 Chemotaxis in bacteria. *Science* **153**, 708–716. (doi:10.1126/science.153.3737.708)
42. Flemming HC, Wingender J. 2010 The biofilm matrix. *Nat. Rev.* **8**, 623–633.
43. Cross MC, Hohenberg PC. 1993 Pattern formation outside of equilibrium. *Rev. Mod. Phys.* **65**. (doi:10.1103/RevModPhys.65.851)
44. Homsy GM. 1987 Viscous fingering in porous media. *Annu. Rev. Fluid Mech.* **19**, 271–311. (doi:10.1146/annurev.fl.19.010187.001415)
45. Paterson L. 1981 Radial fingering in a Hele Shaw cell. *J. Fluid. Mech.* **113**, 513–529. (doi:10.1017/S0022112081003613)
46. Langer JS. 1980 Instabilities and pattern formation in crystal growth. *Rev. Mod. Phys.* **52**, 1–30. (doi:10.1103/RevModPhys.52.1)
47. Wakita J, Itoh H, Matsuyama T, Matsushita M. 1997 Self-affinity for the growing interface of bacterial colonies. *J. Phys. Soc. Jpn* **66**, 67–72. (doi:10.1143/JPSJ.66.67)
48. Ford RM, Lauffenburger DA. 1991 Analysis of chemotactic bacterial distributions in population migration assays using a mathematical model applicable to steep or shallow attractant gradients. *Bull. Math. Biol.* **53**, 721–749. (doi:10.1007/BF02461551)
49. Zhou S, Lo WC, Suhalim JL, Digman MA, Gratton E, Nie Q, Lander AD. 2012 Free extracellular diffusion creates the Dpp morphogen gradient of the *Drosophila* wing disc. *Curr. Biol.* **22**, 668–675. (doi:10.1016/j.cub.2012.02.065)
50. Yu SR, Burkhardt M, Nowak M, Ries J, Petrášek Z, Scholpp S, Schwille P, Brand M. 2009 Fgf8 morphogen gradient forms by a source–sink mechanism with freely diffusing molecules. *Nature* **461**, 533–537. (doi:10.1038/nature08391)
51. Ben Amar M. 2013 Chemotaxis migration and morphogenesis of living colonies. *Eur. Phys. J. E* **36**, 64. (doi:10.1140/epje/i2013-13064-5)
52. Ziebert F, Aranson IS. 2013 Effects of adhesion dynamics and substrate compliance

on the shape and motility of crawling cells. *PLoS ONE* **8**, e64511. (doi:10.1371/journal.pone.0064511)

53. Tindall MJ, Maini PK, Porter SL, Armitage JP. 2008 Overview of mathematical approaches used to model bacterial chemotaxis II: bacterial populations. *Bull. Math. Biol.* **70**, 1570–1607. (doi:10.1007/s11538-008-9322-5)
54. Eberl HJ, Parker DF, van Loosdrecht MCM. 2001 A new deterministic spatio-temporal continuum model for biofilm development. *J. Theor. Med.* **3**, 161–175. (doi:10.1080/10273660108833072)
55. Roca-Cusachs P, Sunyer R, Trepat X. 2013 Mechanical guidance of cell migration: lessons from chemotaxis. *Curr. Opin. Cell Biol.* **25**, 543–549. (doi:10.1016/j.ceb.2013.04.010)
56. Cochet-Escartin O, Ranft J, Silberzan P, Marcq P. 2014 Border forces and friction control epithelial closure dynamics. *Biophys. J.* **106**, 65–73. (doi:10.1016/j.bpj.2013.11.015)
57. Klapper I, Rupp CJ, Cargo R, Purvedorj B, Stoodley P. 2002 Viscoelastic fluid description of bacterial biofilm material properties. *Biotechnol. Bioeng.* **80**, 289–296. (doi:10.1002/bit.10376)